ChemElectroChem

Chemistry Europe
European Chemical Societies Publishing

Title: Constructing Ion-Selective Coating Layer with Lithium Ion Conductor LLZO and Binder Li-Nafion for Separator Used in Lithium-Sulfur Batteries

Authors: Boyang Huang, Haiming Hua, Pengbin Lai, Xiu Shen, Ruiyang Li, Zheng He, Peng Zhang, and Jinbao Zhao

To be cited as: *ChemElectroChem* **2022**, e202200416

Link to VoR: https://doi.org/10.1002/celc.202200416

WILEY-VCH

Constructing Ion-Selective Coating Layer with Lithium Ion Conductor LLZO and Binder Li-Nafion for Separator Used in Lithium-Sulfur Batteries

Boyang Huang,[a] Haiming Hua,[a] Pengbin Lai,[a] Xiu Shen,[a] Ruiyang Li,[a] Zheng He,[b] Peng Zhang,*[b] Jinbao Zhao*[a]

Abstract: In the study of lithium-sulfur batteries, the shuttle effect of polysulfide ions is widely regarded as the most critical factor in the battery performance deterioration. In this article, with the strategy of ion-selection, a method of preparing a coating layer with solid-phase conduction for a separator is used to suppress such an effect. The coating layer is based on calcined ceramic $Li_7La_3Zr_2O_{12}$ (LLZO) and formed through a simple coating method to be thin but dense. The gap between particles is filled with lithiated Nafion (Li-Nafion) which can block polysulfide ions through coulombic interactions of sulfonate groups and allow the lithium ion conduction. The properties of compactness and the ion-selection form a double barrier effect, manifested as the fact that the estimated lithium ion transport number achieves 0.79. Correspondingly, the lithium-sulfur batteries assembled with the ion-selective conduction separators have better lithium deposition behavior and exhibit brilliant cycling performances and capacity retention.

Introduction

With the gradual exhaustion of fossil energy, a reality lies before humanity that we are facing a new round of energy crises. While there have been many attempts to develop new types of energy, such as solar energy, nuclear energy, and wind power, it is also essential to break through the bottleneck of energy storage technology. Rechargeable batteries are an important means for efficient conversion of electrical energy and bring lots of convenience in modern times. Its application is so widespread that it can be seen in a cardiac pacemaker, a mobile phone, a laptop, or even an electric vehicle, and the use of lithium batteries is the most prominent among them. With the development of relevant technology, the issue of energy density has received constant attention, and the demand for higher specific energy continues to expand.[1]

Considering the cathode sulfur has an extremely high theoretical specific capacity of over 1600 mAh g^{-1} and once it is paired with anode lithium metal, the lithium-sulfur battery has the potential to be an alternative energy storage system outside existing ones.[2] Though the value of cathode specific capacity looks very attractive, there are still various difficulties to overcome in the development of lithium-sulfur batteries. Generally, it is summarized into three obstructions. Firstly, the electronic conductivity of the elemental sulfur is not good at all, so more conductive agents need to be added when preparing electrodes, which reduces the overall energy density. Secondly, the volumetric expansion for the sulfur taking a conversion reaction to lithium sulfide (Li_2S) may affect the electrode architecture, which in turn affects the reversibility of the charging / discharging process. Moreover, the most severe problem is the “shuttle effect,” which means the dissolution of soluble intermediate polysulfides and their shuttle from cathode to anode, causing the corrosion of lithium anode and the decrease of the coulombic efficiency and the utilization for a sulfur cathode.[3]

From the perspective of the constructions for lithium-sulfur batteries, the efforts to suppress the shuttle effect could be classified as cathode modification, anode protection, separator modification, or electrolyte additive, among which the electrolyte additive lithium nitrate ($LiNO_3$) gets the most extensively used, and the cathode modification is regarded as the most typical strategy.[4] In terms of chemical interaction, some metal oxides, metal sulfides, and conductive polymers have enough strong bonding energy to immobilize polysulfides;[2b, 5] in terms of physical adsorption, some specific structure was used to absorb polysulfide ions, such as micropores and hollow sphere structures.[6] Although the mix of sulfur and corresponding materials might be compelling due to the usually stronger chemical interaction, it is commonly more useful to form a layer to maximize the utilization of related substances, especially an interlayer between cathode and separator.[7]

For a battery, the separator plays a vital role in the energy conversion process as well as the safety of the cell because it isolates the cathode from the anode and permits the transport of ions in the electrolyte. As for a lithium-sulfur battery, in addition to the above requirements, the demand for blocking the shuttle of polysulfide ions makes the modification of the separator become one of the focuses of related research.[7a, 8] Considering the cost of research, coating modification on widely used commercial polypropylene (PP) and polyethylene (PE) membranes to form a layer between cathode and separator seems a better choice. Typical coating materials for lithium-sulfur batteries include carbon materials, inorganic particles, organic polymers, and multi-component composites, representatively conductive carbon, carbon nanofibers, graphene, alumina, ruthenium (IV) oxide, lithium fluoride, Nafion, etc.[9]

[a] B.-Y. Huang, H.-H. Hua, P.-B. Lai, X. Shen, R.-Y. Li, Pro. J.-B. Zhao
College of Chemistry and Chemical Engineering, State-Province Joint Engineering Laboratory of Power Source Technology for New Energy Vehicle, State Key Laboratory of Physical Chemistry of Solid Surfaces, Engineering Research Center of Electrochemical Technology, Ministry of Education, Collaborative Innovation Centre of Chemistry for Energy Materials, Xiamen University, P.R.China.
E-mail: jbzhao@xmu.edu.cn;
[b] Z. He, Dr. P. Zhang
College of Energy & School of Energy Research, Xiamen University, Xiamen 361005, P.R. China.
E-mail: pengzhang@xmu.edu.cn

Supporting information for this article is given via a link at the end of the document.

Besides, the application of solid electrolytes, which simultaneously play a dual role of separator and electrolyte, is also regarded as another strategy. In a gel polymer electrolyte system with polymer matrix plasticized by liquid electrolyte, similar to the case in a normal liquid-phase lithium-sulfur battery, the problems such as the shuttle effect still exist. While in an all-solid electrolyte system, although the solid-phase ionic conduction could avoid the shuttle effect of intermediate polysulfides, the related research is constrained by low ionic conductivity and interface contact to apply in practical conditions, whether it is solid polymer electrolytes, inorganic solid electrolytes, or organic-inorganic composite solid electrolytes. However, in the solid and quasi-solid state, the shuttle effect of polysulfide ions is intrinsically not significant after all.[9j, 10] The previous research on the immobilization of anions in single-ion conducting solid electrolytes could be an inspiration: the anions can be fixed on the backbone of polymers or in the lattice of inorganic electrolytes as much as possible in our research of the separator coating layer to form solid-phase or quasi-solid-phase conduction which is close to the single-ion conduction of lithium ions. In single-ion conductive polymers, this ion-selective effect increases the Li^+ transport number; and in lithium-sulfur batteries, the ion-selectivity would additionally immobilize polysulfide anions in the liquid phase.

Among various lithium ion conducting inorganic substances, garnet ceramic $Li_7La_3Zr_2O_{12}$ (LLZO) is recognized as a representative because of its good performance and chemical stability. In theory, the pathways of lithium ion diffusion in inorganic electrolytes could be random to some extent, but there is a proven mechanism that lithium ions can hop between the octahedral sites in garnets to migrate. In garnet ceramic LLZO, the route is based on shared triangular faces of the octahedral and tetrahedral sites, and its corresponding activation energy is evaluated as 0.26 eV by ab initio calculations. The low energy barrier implies that LLZO could provide the lithium ion conduction with relatively higher ionic conductivity.[11] Normally, LLZO is calcined into ceramic sheets to produce inorganic solid electrolytes, but the high-temperature calcination step is unpractical for the modification of commercial separators. Then the idea of preparing composite solid electrolytes with LLZO and polymer was naturally thought of, and the composite coating layer was designed with the main component LLZO and a small but moderate amount of polymer. Under the premise of choosing a suitable polymer, it would be possible to achieve solid-phase or quasi-solid-phase conduction in the LLZO ceramic coating layer.[12]

Due to high proton conductivity and excellent stability, perfluoro ionomer Nafion has been widely used in proton exchange membrane fuel cells. In the view of its structure, it has a backbone of polytetrafluoroethylene (PTFE) and a side chain of perfluorosulfonic acid, in which the former means better stability and the latter provides the possibility of functionalization. Nafion and its lithiation product lithiated Nafion (Li-Nafion) both have the feature of allowing the Li-ion transport and rejecting the polysulfide anions diffusion, which is the function conferred by the coulombic interactions of sulfonate groups. It could not only form a coating layer or a film alone due to its film-forming properties but also could be used as a binder for sulfur cathode or an interlayer. When used as a binder, Nafion and Li-Nafion could form a dense structure that prevents the electrolyte from rapidly permeating into the bulk phase, making the ion transport in the coating layer close to the solid phase.[13]

In our study, a dense coating layer on the surface of a commercial PE separator with LLZO and Li-Nafion in 2 μm thickness was formed, in which LLZO was the main component after being calcined to remove impurities and Nafion was fully lithiated to form Li-Nafion as the binder. As the graphical abstract in Figure 1 shows, LLZO provided the lithium ion conductivity, and Li-Nafion filled the gaps between LLZO particles to firmly bond LLZO and manufacture dense layer while blocking the migration of polysulfide ions. Under the synergistic effect of the two components, the ionic conduction in the coating layer exhibits selectivity. That is to say, the lithium ion transport in the coating layer was close to single-ion conduction in the solid phase, and at the same time, the shuttle effect of polysulfides in lithium-sulfur batteries was successfully suppressed. Manifested as a lower cycle decay value of the battery and uniform deposition morphology of lithium metal, this synergistic effect was confirmed to exist. Appropriate characterization methods such as polysulfide permeation measurements, ^7Li Nuclear Magnetic Resonance (NMR) spectroscopy, and X-ray photoelectron spectroscopy (XPS) S 2p spectra proved that this method of providing conducting and blocking features separately through the rational design of composite materials was practical and effective, which could build the ion-selective conduction in solid phase or quasi-solid phase.

Results and Discussion

The design idea of this research is given in Figure 1. Before preparing modified separators, it was necessary to ensure the purity of all the materials, especially the lithiated Nafion (Li-Nafion) and the calcined ceramic $Li_7La_3Zr_2O_{12}$ (LLZO). For the lithiated process of Nafion, attenuated total reflection Fourier transform infrared spectroscopy (ATR-FTIR) spectra and thermogravimetric & differential scanning calorimetry (TG & DSC) measurements were used to distinguish H^+ form Nafion (H-Nafion) membrane and lithiated Nafion (Li-Nafion) membrane, shown in Figure 2. By comparing the ATR-FTIR spectra before and after lithiation, it could be found that there are mainly two peaks that have shifted: The peak at around 1710 cm^{-1} is the result of the bending band of the hydrated proton in H-Nafion; it moved to 1640 cm^{-1} after lithiation due to the replacement of H^+ by Li^+; the peak at about 1050 cm^{-1} could be attributed to the $-SO_3^-$ symmetric stretch band, it moved to a higher wavenumber, indicating that there was a new interaction between Li^+ and oxygen establishing after the lithiation.[9n, 14] It leads to the conclusion that the method of lithiating in LiOH solution is reliable, and Li^+ successfully substituted H^+ in our experiment.

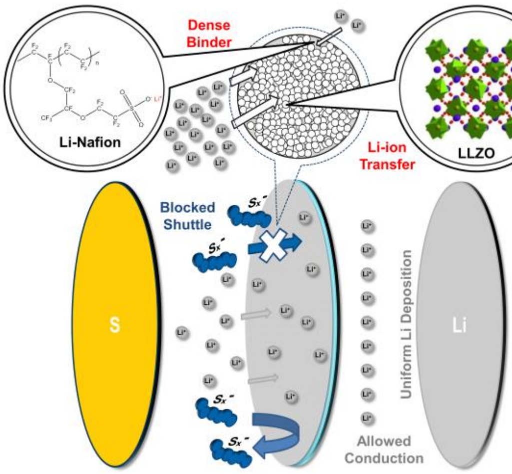

Figure 1. Graphical abstract of this research

In Figure 2b, in the TG curves, the weight loss of H-Nafion starts before 300 °C while the weight loss of Li-Nafion appears after 400 °C; in the DSC curves, there are two endothermic peaks for H-Nafion at about 300 °C and 450 °C while there is only one endothermic peak for Li-Nafion at around 450 °C. The reason for the differences is that there were two steps in the thermal decomposition of H-Nafion corresponding to the sulfuric acid groups and the main chains, while there was only one step, the splitting-off of main chains left in Li-Nafion. In other words, the bonding between H^+ and oxygen is weaker, so the sulfuric acid tended to decompose at a lower temperature, and when the interaction turns to be Li^+ and oxygen, the temperature of decomposition would be delayed.[15] The result of TG & DSC curves is another proof of the substitution of H^+ and additionally implies that Li-Nafion has better thermal stability than H-Nafion.

As for the ceramic LLZO, as we know, the garnet electrolyte LLZO has poor air stability and trends to have reactions to generate Li_2CO_3 impurity, whether it is a single-step reaction pathway with dry CO_2 or a reaction pathway including LiOH formation.[16] So the fresh ceramic LLZO was used immediately after the final synthesis step 1000 °C calcination to avoid the generation of Li_2CO_3 contaminant as much as possible. Besides, the X-ray diffraction (XRD) pattern was used to detect the bulk structure of LLZO that we used in the experiments, shown in Figure 2c. Compared with the standard cubic-LLZO phase pattern (PDF 00-063-0174, $Li_7La_3Zr_2O_{12}$) and the simulation result in Module Reflex Powder Diffraction of Software Materials Studio,[17] the result of XRD coincides with the standard pattern and has no impurity peak, especially at 21.3° and 31.8° which are commonly regarded as the characteristic peaks of Li_2CO_3 impurity in LLZO. Considering that a phase change usually accompanies the deterioration of LLZO in the air, it goes to the conclusion that the purity of LLZO used in the research is acceptable.

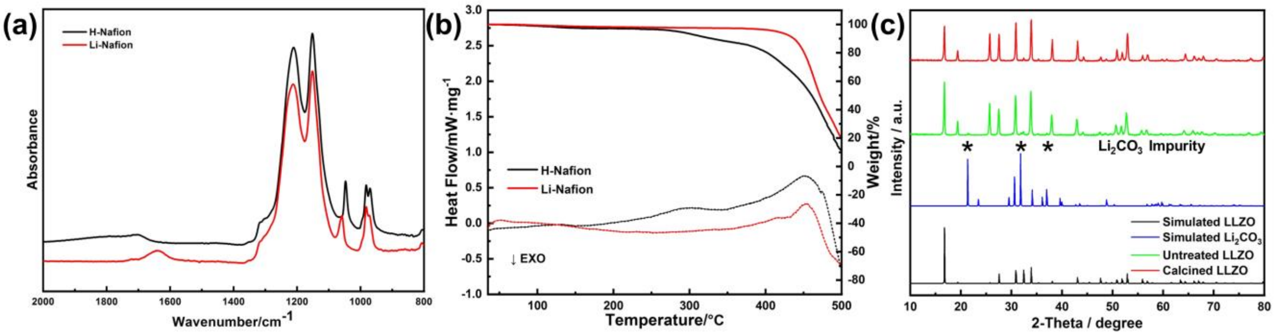

Figure 2. Characterizations of raw materials: (a, b) ATR-FTIR spectra and TG & DSC curves before and after the lithiation of Nafion; (c) XRD patterns of LLZO and possible impurity Li_2CO_3

Considering that a single LLZO particle could be quickly excited by voltage and be captured with a blurred image in the field emission scanning electron microscopy (FE-SEM) and energy dispersive X-ray spectroscopy (EDS) characterization, more information about LLZO could be obtained in the FE-SEM images and EDS results of the ceramic coating separators after preparation of separators whose binder of the ceramic layer were H-Nafion (L-HN) and Li-Nafion (L-LN), shown in Figure 3 and Figure S1. The method of preparing ceramic coating separators was a part of our previous work, and it was not hard to control the properties of the ceramic layer.[18] In the FE-SEM images of surfaces (Figure 3a, 3b, S1a and S1b), it could be seen that the coating ceramic is mainly LLZO with binder H-Nafion or Li-Nafion filling in between and looks pretty dense and uniform, and the surface of the coating layer was fairly flat with few pores, which could be filled by liquid electrolyte. LLZO maintained its irregular ceramic particle morphology after the coating process, with an average diameter of about 500 nm, consistent with the manufacturer's parameters; the binder fills the gaps of LLZO particles and is tightly coupled bonded to form a continuous and uninterrupted layer. This kind of ceramic layer could create effective physical isolation by solid-state conduction and interrupt the shuttle effect of polysulfide ions, while it might not block the migration of lithium ions due to the fast transmission in LLZO for lithium ions.[11b, 11c] In the FE-SEM images of cross-sections (Figure 3c, 3d, S1c and S1d), the thickness of the coating layer could be obtained by the electron microscope scale. It is relatively thin, about 2 μm, ensuring that it is not tricky for lithium ions to transmit through the separator, and it is difficult for LLZO particles to be completely separated in the layer. The EDS spectra in Figure 3e and S1e help understand each component's existence form in the ceramic layer. For the coating layer, its ingredients are mainly LLZO particles, shown by the element La which is distributed in a large amount correspondingly; while for a single LLZO particle with typical ceramic morphology, it is tightly wrapped by Li-Nafion to achieve adhesive bonding, proved by the bright field of element C and F around the ceramic particle. To conclude, as for the coating properties, it might provide single-ion and solid-phase conduction for lithium ions and meets our expectations for a ceramic layer that is able to provide ion-selectivity, in other words, allowing lithium ions and prohibiting polysulfide ions from passing through it.

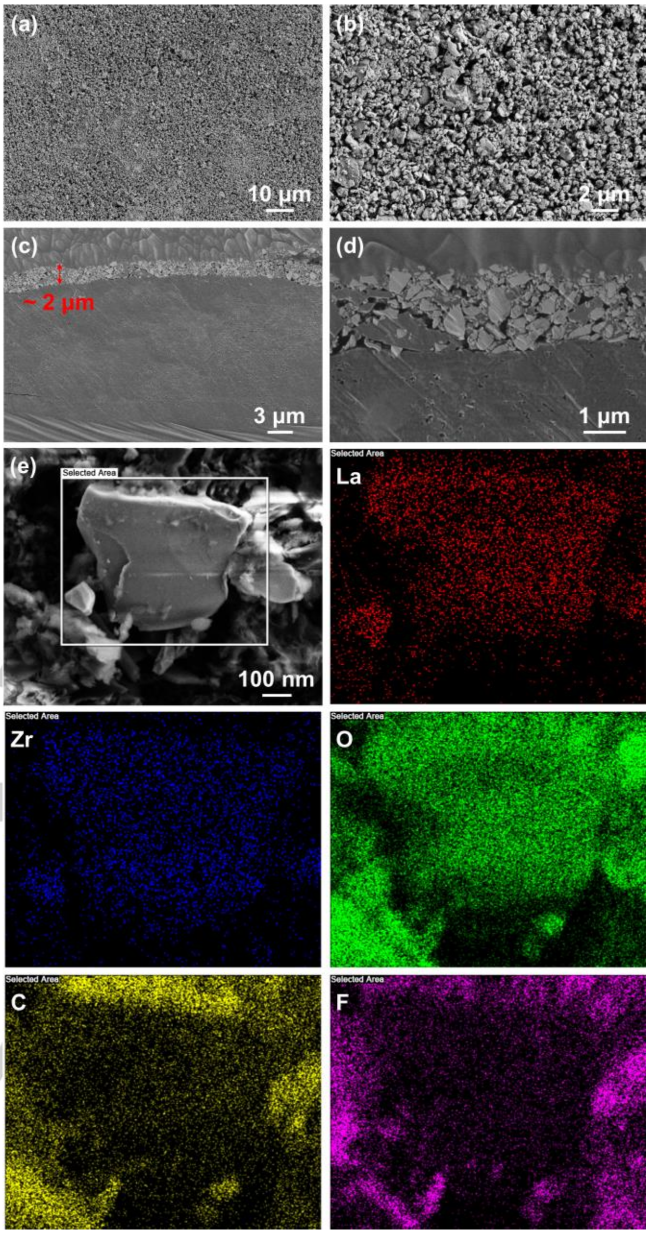

Figure 3. Microscopic morphology of ceramic coating layer and individual LLZO particles: (a, b) surface FE-SEM images of L-LN separator; (c, d) cross-sectional FE-SEM images of L-LN separator; (e) EDS spectra of individual LLZO particle

In Table 1, for basic features of the separators, some experiments were carried out, and it was found that there were two indicators for L-HN and L-LN separators that were different from ordinary ceramic coating separators. For a normal coating process of commercial ceramic coating separators, in consideration of the existence of an additional layer, the Gurley value will increase to a certain extent, but usually not more than 500 seconds for 100mL gas. At the same time, the contact angle will become much smaller after manufacture due to the lyophilicity of the ceramic particles. However, for L-HN and L-LN separators, the Gurley values for these two kinds of separators had sharply increased and exceeded 600 s for 100 mL air, which implied a remarkable decrease in air permeability. Besides, the contact angles became respectively about 41° and 42°, not much different from the initial value of 46° of pristine PE, meaning that the electrolyte dripped to the surface of separator no longer quickly penetrated from the ceramic layer. Considering that LLZO is not a non-lyophilic ceramic, this phenomenon could be regarded as one of the shreds of evidence that the ceramic layer is dense enough to make the electrolyte penetrate slowly, consistent with the results of FE-SEM images.

Table 1. Physical properties of PE, Nafion, L-HN, L-LN

Separator	PE	Nafion	L-HN	L-LN
Thickness (μm)	20	50.8	22	22
Contact angle (°)	46	44	41	42
Electrolyte uptake (%)	52	41	61	58
Porosity (%)	44.2	30.6	41.8	41.6
Gurley value (s 100mL^{-1})	229	>1800	644	657

Then the electrochemical properties of the separators were tested, including linear sweep voltammetry (LSV), electrochemical impedance spectroscopy (EIS), and Li$^+$ transport number (t_{Li}^+). The chemical stability of the separators soaked in the electrolyte was characterized by the LSV test for a Li / separator / stainless steel semi-blocking cell. In the field of lithium-sulfur batteries, ether electrolytes are widely studied; in this work, the most common type of electrolytes, 1 M LiTFSI dissolving in a mixture of DME and DOL, was used. Limited by the voltage stability of ether solvents, it is difficult for the electrolyte to withstand high voltage, and the upper limit of the electrochemical window is usually lower than 4 V.[19] This phenomenon is also reflected in Figure 4a, and there starts to have a current at about 4.2 V when using stable pristine PE separators. As for the Nafion, L-HN, and L-LN separators, the curves are similar to the above situation, and there is no peak at 0 V to 4 V. In view of the voltage range in our study from 1.8 V to 2.6 V, it is rational to say that there was no significant change in the electrochemical window before and after coating and all the separators could stably exist in the ether electrolyte window without side reactions.

To understand the role of the coating layer played in lithium ion transport, simulating cells with two lithium foils were assembled, and then potentiostatic polarization was given with a constant potential of 10 mV. In Figure 4b, 4c, 4d and 4e, the current slowly went down, and the initial and final impedance fitted with the equivalent Randles circuit were ultimately different. Through the formula given in the Electrochemical Measurements part, the t_{Li}^+ could be evaluated to be 0.28, 0.65, 0.68, and 0.79 for different separators. For commercial PE separators, the transmission of positive and negative ions was not restricted, and the t_{Li}^+ is usually considered to be in the range of 0.2 to 0.4. When Nafion separators used, the polysulfides were blocked to hinder the transport of negative ions, making t_{Li}^+ rise to 0.65, which is consistent with the previous literature.[9n, 13c] For L-HN separators, compared with pure Nafion separators, the added LLZO ceramic might slightly reduce the compactness. However, LLZO is a kind of enough good lithium ion conductor, making the proportion of lithium ion conduction further increased. As for L-LN separators, the proton of Nafion was replaced by Li$^+$, and there was no longer proton migration in positive ion migration. The t_{Li}^+ finally became 0.79, which is close to the situation of a single-ion conductor.[13a, 13d, 14b] For lithium-sulfur batteries, in the case of less impact on electrochemical impedance, with the solid-phase conduction in the ceramic coating layer, as the result of constructing an ion-selective layer, a high Li$^+$ transport number means polysulfide ions tend to be successfully restricted, which is the base for our research.

Electrochemical impedance spectroscopy (EIS) for a separator was used to characterize the influence of the coating process, shown in Figure 4f, 4g and Table 2. We tested the electrical resistance of the separators soaked with electrolyte, calculated the ionic conductivity in combination with the physical properties, and finally evaluated the Li$^+$ ionic conductivity based on the t_{Li}^+ above. As we know, the Nafion membrane itself is very dense and cannot conduct lithium ions quickly, which was reflected in the result that the electrochemical impedance has risen by nearly one order of magnitude.[9n] When LLZO ceramic was used as the coating component, the overall resistance increase was not apparent due to its rapid lithium ion conduction characteristics, and the final Li$^+$ ionic conductivity was roughly the same order of magnitude as that of commercial PE separators. This result makes the L-LN membrane possible to be used in the batteries with a relatively larger rate, and in this situation, the uniform LLZO coating might play a role in inducing uniform deposition of lithium metal to immigrate serious lithium dendrites.[20]

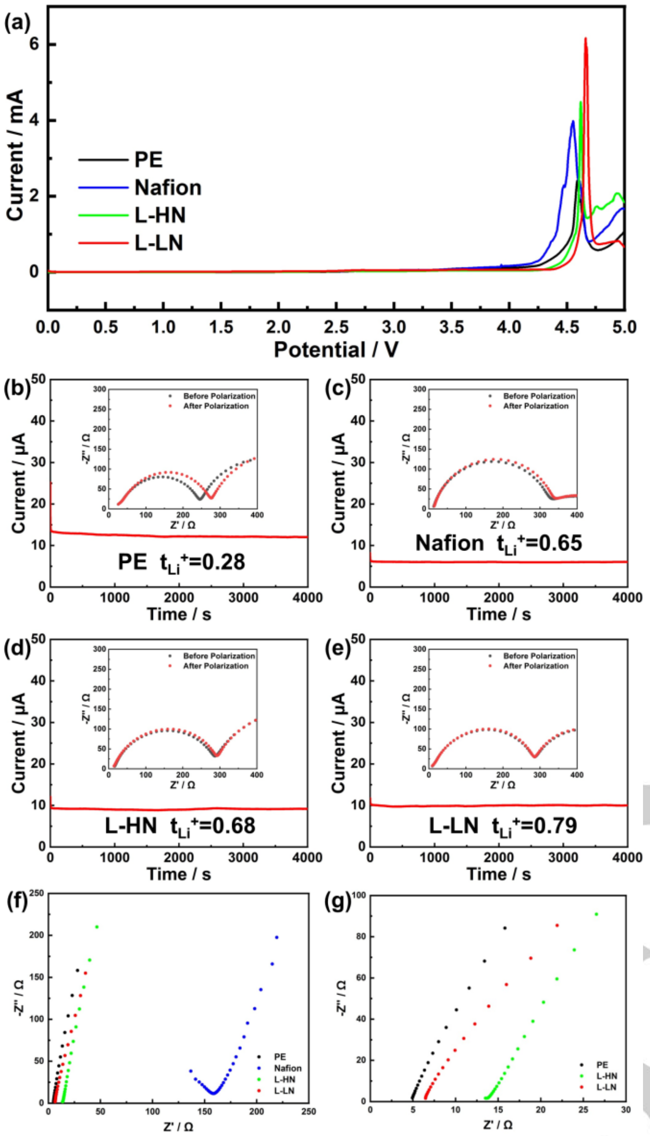

Figure 4. Electrochemical properties of separators: (a) LSV curves of different separators soaked in ether electrolyte; (b-e) Li$^+$ transport number for different separators; (f, g) EIS tests for different separators soaked in ether electrolyte

Table 2. Properties for conductivity of PE, Nafion, L-HN, L-LN

Separator	PE	Nafion	L-HN	L-LN
Impedance (Ω)	4.94	158.67	13.61	6.48
Ionic conductivity (S cm^{-1})	2.86×10^{-4}	1.59×10^{-5}	8.03×10^{-5}	1.69×10^{-4}
t_{Li}^+	0.28	0.65	0.68	0.79
Li$^+$ ionic conductivity (S cm^{-1})	8.01×10^{-5}	1.03×10^{-5}	5.46×10^{-5}	1.34×10^{-4}

In the part of the battery test, the above conjecture seemed to be verified from the side. From the voltage of 1.8 V to 2.6 V, the 2016 coin cells with different separators were tested on a Neware battery program-control system. For the short-term cycling performance in Figure 5a, respectively, the initial discharge capacities were 1174.8, 1145.5, 1067.1, and 1032.7 mAh g^{-1}, discharge capacities after 100 cycles were 801.2, 702.8, 565.7 and 449.4 mAh g^{-1}, and the capacity retentions were 68.2, 61.4, 53.0 and 43.5 %. The batteries with L-LN separators showed better cycling performances as expected, and the charge / discharge curves of certain cycles were given in Figure 5b, with typical voltage plateaus for lithium-sulfur batteries. The loss discharge of capacity in the first few battery cycles could mainly be regarded as the irreversible loss caused by the dissolution of polysulfides, and there was also a capacity loss caused by the shuttle effect of polysulfide ions, mainly reflected in the fade away of capacity in subsequent battery cycles. For the former capacity loss, the impact of the L-N separator was not very significant; but for the latter, the inhibitory effect of the L-N separator was evident, embodied in steady discharge capacity after 10 battery cycles.[21] Compared with the situation in other batteries, obviously, the steady capacity was not the dissolution saturation but the dissolution inhibition of polysulfide ions. With an increased loading in Figure 5c, the capacity retention of 100 cycles for the L-LN separator was still acceptable 62.8 %. Shown in Figure 5d, compared to the capacity retention of 39.2 % for PE separator, the capacity retention after 200 cycles for L-LN separator was a better value of 56.4 % when the C-rate was raised to 0.5 C. And in Figure 5e, when both the number of cycles and the C-rate increased to respectively 500 cycles and 2 C, the capacity retention for L-LN separator was 51.0 %. Obviously, regardless of the C-rate and the number of battery cycles, the lithium-sulfur batteries with L-LN separators had better cycling performances, which was consistent with our vision as the result of multiple barrier effects in the solid state for composite materials of the ion-selective coating layer.

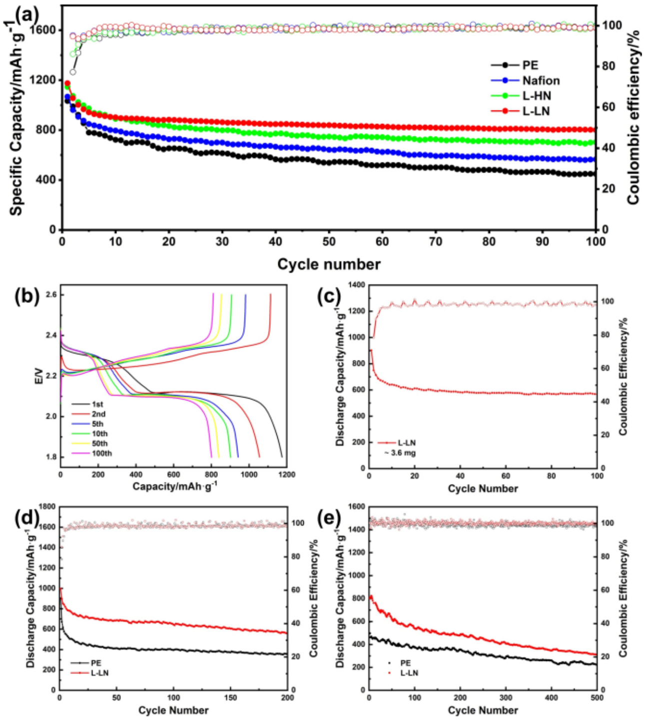

Figure 5. Cycling performances of lithium-sulfur batteries assembled with ether electrolyte and different separators in the voltage range of 1.8 V to 2.6 V: (a, b) cycling performances for different separators and charge / discharge curves for L-LN separator with a sulfur loading 1.2 mg cm^{-2} at 0.2 C; (c) cycling performances for L-LN separator with a sulfur loading 3.6 mg cm^{-2} at 0.2 C; (d) cycling performances for PE and L-LN separator with a sulfur loading 1.2 mg cm^{-2} at 0.5 C; (d) cycling performances for PE and L-LN separator with a sulfur loading 1.2 mg cm^{-2} at 2 C

In order to intuitively understand the barrier ability of the L-LN separator to polysulfide ions, polysulfide permeation measurements were carried out with an H-type tube. In Figure 6, the color of the right chambers for different separators was the same at the beginning. As expected, a color change of the right chambers could be observed after different times for different separators. The right tube with pristine PE separator turned slightly yellow near the clip after just 0.5 h, and after 2 h the yellow became darker and spread to the entire right container rapidly. In contrast, the right chambers with Nafion and L-LN separators could keep clear and transparent for 8 h without turbidity, and the chambers were also only slightly colored when the time was extended to 72 h, which could prove that the L-LN coating layer is able to achieve the similar effect as Nafion membrane in suppressing polysulfide ions, considering that the ability to block polysulfides for Nafion is widely recognized and researched. This kind of physical isolation is one of the reasons why the lithium-sulfur cells with L-LN separators could achieve higher performance in cycling due to the restriction of the diffusion of polysulfide ions.

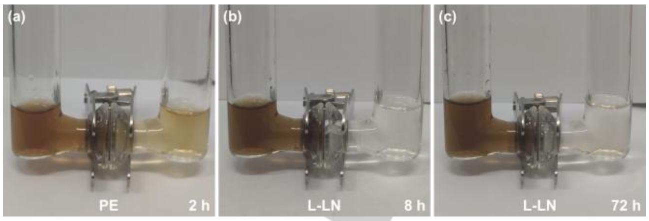

Figure 6. Polysulfide permeation measurements with different separators

To confirm that this physical isolation still worked in the lithium-sulfur batteries with electrochemical reactions, different batteries after cycling were disassembled in a glove box with an argon atmosphere, and each component was studied separately. For the lithium metal foil, FE-SEM characterizations were used to investigate the lithium metal anode before and after battery cycling in our study. In Figure 7a, 7b, 7c and 7d, for the lithium-sulfur cells using commercial PE separators, the surface of the lithium metal foil became quite uneven after 50 cycles. As described in previous literature, the shuttled polysulfide ions might cause lithium metal corrosion in the process of deposition, forming extremely uneven deposition morphology.[22] After 100 cycles in Figure 7e and 7f, even the emergence of hollow lithium metal could be observed, which meant there tended to be many lithium dendrites on the anode due to the severe shuttle effect of polysulfide ions. In contrast, the lithium-sulfur cells using L-LN separators maintained smoother morphologies without abnormal dendrite and irregular holes. There was a very uniform scaly lithium deposition on the lithium anode after 50 cycles, and the scales became larger slices without severe disorder when the number of cycles increased to 100, consistent with the lithium metal deposition at low polysulfide content in previous research.[23] The absence of irregular lithium holes could be understood as the lack of polysulfide ions through the solid-phase interlayer, while the uniform deposition might be caused by the additional inducing effect of uniform LLZO coating.[20] This difference in lithium deposition is a powerful proof that the ion-selective coating layer impacted as we thought, ensuring that the corresponding batteries achieved better electrochemical performance as the former part of the battery test showed.

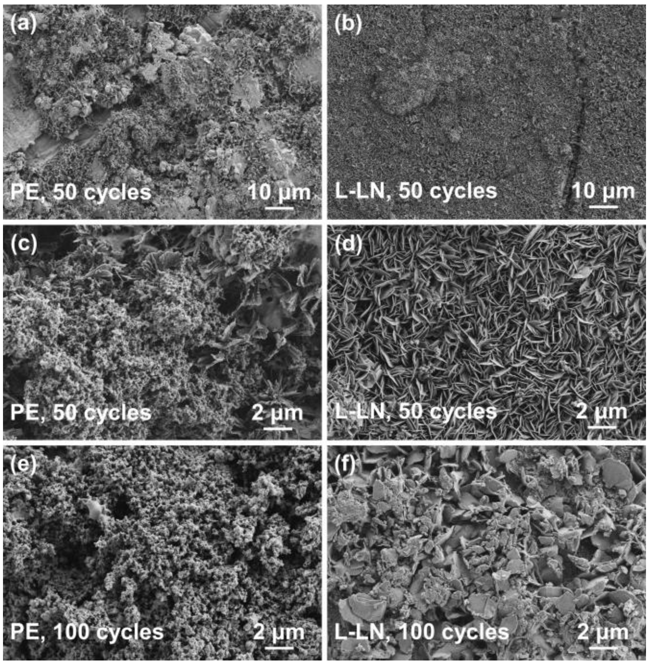

Figure 7. Microscopic morphology of lithium metal foil for different separators and different battery cycles

For the separators in disassembled batteries, the X-ray photoelectron spectroscopy (XPS) S 2p spectra of the surface of separators towards lithium metal anode could directly give relevant evidence of the form of existence of sulfur. In the previous reports, the peaks were analyzed by fitting program, and the type of substance and the peak position are corresponding to the following within the allowable range of error: LITFSI - 169.6 eV, S (IV) - 167.6 eV, Bridging S - 163.0 eV, Terminal S - 161.5 eV and Li_2S - 160.0 eV.[24] According to the criterion of peak differentiating and imitating for p energy level, peak fitting results were shown in Figures 8a and 8b. As we know, the peaks of bridging S and terminal S in the spectra corresponded to long chained polysulfides, which seemed stronger for pristine PE separator and meant the process of passing through the separator to the anode for polysulfides. For the L-LN separator, little bridging S and terminal S could be found due to the suppressed shuttle of polysulfide ions. In other words, in the process of diffusion for polysulfide ions through a solid-state ceramic coating layer, although there was still a bit of polysulfide that shuttled from the cathode side to the space between the separator and the anode, the degree of the shuttle was greatly limited, so that the ion-selective coating layer did play a role in blocking anions and corresponding batteries could show better performance as a consequence.

Besides, for the electrolyte in disassembled cells, the ^{7}Li NMR spectroscopy of the electrolyte provides another side of evidence. For the electrolyte near the anode side, samples were taken carefully and used in the external standard method described in our previous study to avoid the influence of added deuterated solvents and reduce the contact between air and electrolyte.[18b] Shown in Figure 8c, the pristine ether electrolyte had a peak at -0.82 ppm, which was regarded as the characteristic peak of LiTFSI. After battery cycles, the content of polysulfides near the anode electrode increased, and the existing form of lithium was gradually transformed into long chained polysulfide ions. As the ^{7}Li NMR spectroscopy reflected the average form of lithium element, the corresponding peak moved to the positive direction.[25] For the PE separator, the peak shifted to -0.52 ppm after 100 battery cycles, while the number was just -0.65 ppm for the L-LN separator, indicating that less lithium has undergone a change in its existing form and the amount of polysulfides was reduced between the separator and anode, which reflected that our ion-selection strategy efficiently inhibited the shuttle effect.

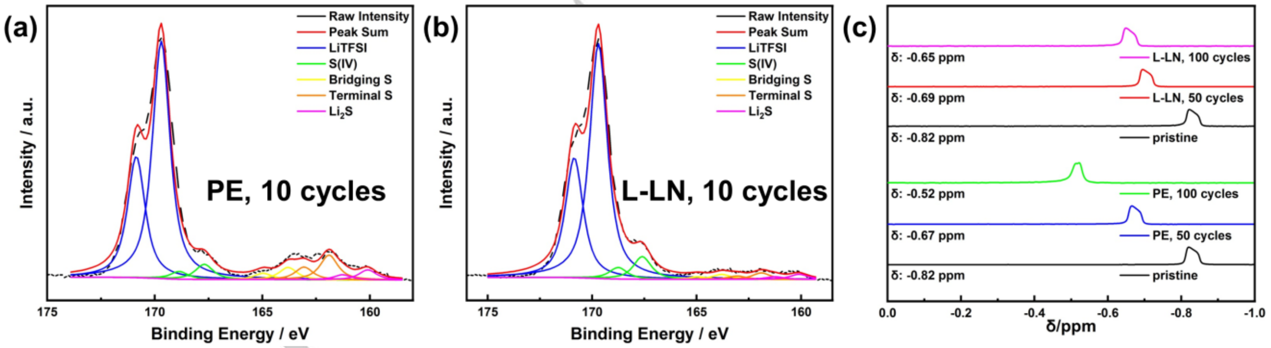

Figure 8. (a,b) XPS S 2p spectra of the surface towards anode for different separators in disassembled batteries, (c) ^{7}Li NMR spectroscopy of electrolytes near the anode side in disassembled batteries

On the site of the compactness and ion-selectivity of the coating layer, its function of blocking polysulfide ions could be explained by the solid-state conduction. However, the mechanism of suppressing the shuttle effect might not only be physical isolation. Considering the coulombic interactions of sulfonate groups reported in the previous literature, it might be synergistic with the effect mentioned above even if the amount of Li-Nafion was not significant for the L-LN separator in this work.[9n, 9o, 13c] In order to verify the existence of this coulombic interaction which was essentially a change in charge, the LLZO particles were scraped from the ceramic layer and distributed in a mixture of DME and DOL by a volume ratio of 1:1 to test the ζ potential. As shown in Table 3, the ζ potential value for pristine calcined LLZO particles was 5.02 mV, which was close to the value stated in the literature.[26] It could be seen that the pristine LLZO particles were basically neutral with a weak positive charge on the surface of the electrolyte. However, for the LLZO scraped from the L-LN separators, the ζ potential sharply decreased to -16.18 mV, similar to the result of low concentration Nafion dispersed in a solvent regarded as dispersion of aggregates.[27] According to the mass ratio of substances in the slurry, two other samples were measured in specific concentrations. From the results, it could be inferred that the existence of Li-Nafion made the ζ potential of the solution negative, which was the basis for charge repulsion. Corresponding to the LLZO scraped from the L-LN separators when Li-Nafion was wrapped on the surface of LLZO, the zeta potential was more negative than in the case where the two components were separately added. It could be further conjected that even a tiny amount of Li-Nafion in the coating layer was able to impart a negative charge, thereby repelling the same negatively charged polysulfide ions. These coulombic interactions and the aforementioned effects - solid-state conduction, uniform deposition, lithium ion conduction, and density - worked together to get multiple barrier effects and ion-selectivity, making lithium-sulfur batteries have better electrochemical performances.

Table 3. Comparison of ζ potentials for different solutions

Samples	ζ potential (mV)
Pristine LLZO (1.8 wt %)	5.02
LLZO scraped from L-LN separator (2 wt %)	-16.18
Li-Nafion (0.2 wt %)	-17.54
Pristine LLZO (1.8 wt %) + Li-Nafion (0.2 wt %)	-10.96

Conclusions

In summary, the strategy of ion-selective solid-phase conduction was used in this work, and a ceramic-coated separator with composite materials of lithium ion conductor LLZO and binder Li-Nafion was manufactured by a simple coating method and applied in lithium-sulfur batteries. After confirming the purity of each component, the compactness of the coating layer was verified by various characterizations. The selective conductivity for lithium ion was brought by the solid-phase mass transfer in the ceramic coating layer and proved by the measurements of the Li^+ transport number. In polysulfide permeation measurements, the related phenomenon of color change could be observed, intuitively reflecting a kind of physical isolation that was beneficial to the cycling performances of lithium-sulfur batteries. However, beyond the dense and lithium ion conductive features of the coating layer, the factors conducive to battery cycling also included the uniform deposition of lithium metal led by uniform LLZO coating, and the coulombic interactions contributed by Li-Nafion. A correct understanding of the function of each component is very necessary for the design of composite materials, and the focus of the study is also based on this. The present study is believed to give a new view on the use of lithium ion conductors in lithium-sulfur batteries as well as to provide a proper perception of a combination of different component functions to suppress the polysulfides shuttle effect in the future research.

Experimental Section

Material Preparation

The H^+ form Nafion (H-Nafion) membrane Nafion 212 (Shanghai Hesen Electrical Ltd.) with a thickness of 50.8 μm was dipped in 1 M LiOH aqueous solution and heated to 80 °C for 12 h to be lithiated. After then, the lithiated Nafion (Li-Nafion) membrane was treated in distilled water at 80 °C for 12 h for washing the residual LiOH solution. The Li-Nafion membrane was vacuum dried at 80 °C for 12 h to remove all the solvent. The change in chemical structure is illustrated in Figure S4.

The ceramic coating separator was prepared on a wet process manufactured PE separator (Asahi Kasei Corp.) substrate. The above-mentioned H-Nafion or the Li-Nafion was used as the binder in the ceramic coating layer. By putting the H-Nafion or the Li-Nafion membrane in anhydrous N, N-dimethylformamide (DMF) at 80 °C for 6 h under a nitrogen atmosphere, the binder H-Nafion or Li-Nafion was dissolved in the solvent DMF, then the 1000 °C calcined ceramic $Li_7La_3Zr_2O_{12}$ (LLZO, Zhangzhou Xiangcheng Yuteng Ceramic Products Co., Ltd.) was added to the solution, and the mass of ceramic / binder / solvent was adjusted to 0.9 g / 0.1 g / 5 g. After ultrasonicated and mechanical stirring mixed, the slurry was applied to one side of the PE separator substrate by an automatic film-coating machine. Then the solvent DMF was removed by drying on a heated plate and in a vacuum oven, as described in our previous work.[18]

Membrane and Material Characterization

The bulk structure of LLZO was characterized by a MiniFlex 600 Benchtop X-ray diffraction device (XRD, Rigaku, Japan), and the result of lithiation was confirmed by Fourier transform infrared spectroscopy (FT-IR) and thermogravimetric & differential scanning calorimetry (TG & DSC) measurements. The FT-IR spectroscopy in the range of 400 – 4000 cm^{-1} was measured by a Nicolet IS5 spectrometer (Thermo Fisher Scientific Inc.), and the TG & DSC measurements with a heating rate of 5 °C min^{-1} from 25 °C to 500 °C were tested by a Model STA 449 instrument (NETZSCH Machinery and Instruments Co., Ltd).

The morphologies of different separators and ceramic particles were investigated with a GeminiSEM 500 field emission scanning electron microscopy (FE-SEM, Zeiss, Germany). An EM TIC 3X triple ion-beam cutter (Leica, Germany) was used to get a flatter cross-sectional surface. The element distributions of different separators were detected with an energy dispersive X-ray spectroscopy (EDS, Zeiss, Germany). The contact angle was measured by a PowereachJC2000C1 contact angle goniometer (Shanghai Zhongchen Digital Technique Equipment Co., Ltd) to weigh the lyophilic ability of surfaces for different separators.

Polysulfide permeation measurements were tested to weigh the permeability of polysulfides for different separators. 0.1 M Li_2S_6 solution was prepared by mixing a corresponding amount of Li_2S and pure sulfur in a 1:1 by volume mixture of dimethoxymethane (DME, anhydrous, Zhangjiagang Guotaihuarong New Chemical Materials Co., Ltd) and 1,3-dioxolane (DOL, anhydrous, Zhangjiagang Guotaihuarong New Chemical Materials Co., Ltd) under 6 h continuous stirring, while the blank solution was just the mixture of DOL and DME. In an H-type electrolytic cell, one chamber was filled with the Li_2S_6 solution, and the other was the blank solution, and a membrane was used to separate the two different solutions and fixed by the chambers and a clamp. After injecting two solutions into two chambers, the color change of the blank solution was observed after a certain period, reflecting the shuttle of polysulfide ions from the Li_2S_6 solution to the other side through the separator.

To further investigate the role of separators in lithium-sulfur batteries, the coin batteries were disassembled in an argon-filled glove box (M. Braun GmbH), and the following components were carefully separated. The X-ray photoelectron spectroscopy (XPS) S 2p spectra of the surface of separators towards anode lithium foil was tested by K-Alpha X-ray photoelectron spectroscopy system (Thermo Fisher Scientific Inc.) and analyzed with the criterion in the previous report to differentiating the peaks of substances.[24] The characterization methods FE-SEM images and EDS spectroscopy were used to observe the morphology and element distributions of the lithium foil before and after battery cycles to verify the influence of the modified separator on lithium deposition. The ^{7}Li Nuclear Magnetic Resonance (NMR) spectroscopy of different electrolytes before and after battery cycles was tested by an AVANCE NEO 500 nuclear magnetic resonance spectrometer (500 MHz, Bruker, USA) through a typical external standard method to explore the existence form of lithium and then to infer the degree of the shuttle of polysulfides. The ζ potential of particles was tested by a ZetaPALS ζ potential analyzer (Brookhaven Instruments Corporation, USA).

Electrochemical Measurements

To investigate the electrochemical stability windows of separators and electrolytes, the linear sweep voltammetry (LSV) from 0 V to 6 V was carried out with the scan rate of 5 mV s^{-1} on a CHI660E electrochemical workstation (Shanghai Chenhua Instruments Limited) for Li / separator / stainless steel semi-blocking cell, in which a lithium foil was used as the reference electrode, and the auxiliary electrode and a stainless steel sheet were used as the working electrode.

On an Autolab electrochemical workstation (Sino-Metrohm Technology Ltd), the electrochemical impedance spectroscopy (EIS) was tested with a frequency range of 0.1 – 10^5 Hz, then the ionic conductivity features of separators could be calculated with the following equation:

$$\sigma = L / (R_b \times A) \quad [1]$$

where σ is the ionic conductivity of the measured separator, L is the thickness of the separator, R_b is the resistance of the system obtained by the EIS test, and A is the contact area of the separator and the electrode.

By potentiostatic polarization method with a simulating cell, the Li^+ transport number (t_{Li^+}) was estimated on a symmetrical battery in which the separator soaked in the liquid electrolyte was put between two lithium foils, using the following equation:

$$t_{Li^+} = I_{SS} (\Delta V - I_0 R_0) / I_0 / (\Delta V - I_{SS} R_{SS}) \quad [2]$$

where ΔV is the constant potential 10 mV, I_0 is the initial current, R_0 is the initial interfacial resistance, I_{SS} is the final current, and R_{SS} is the final interfacial resistance.

The sulfur cathode slurry was prepared by mixing sublimed sulfur (CP, Sinopharm Chemical Reagent Co., Ltd.), acetylene black, and the binder LA132 (Chengdu Indigo Power Sources Co., Ltd) in a mass ratio of 6:3:1 with the solvent deionized water. Then a piece of aluminum foil was selected to be coated with the cathode slurry as mentioned earlier and vacuum dried at 80 °C for 12 h to remove the solvent and prepare the sulfur cathode plate. The mass loading of sulfur was controlled at about 1.2 and 3.6 mg cm^{-2}. The electrolyte was prepared by dissolving 1 M lithium bis(trifluoromethanesulfonimide) (LiTFSI, Zhangjiagang Guotaihuarong New Chemical Materials Co., Ltd) in a mixture of DME and DOL by a volume ratio of 1:1 with 1 wt. % $LiNO_3$ additive. By sandwiching the separator between a lithium foil anode and the sulfur cathode in a glove box and then injecting the electrolyte as mentioned above in the proper amount, a lithium-sulfur 2016 coin cell was assembled with different sulfur loadings. Then on a Neware battery program-control system, the batteries were tested for the cycle performance with the corresponding current rate in the voltage range of 1.8 V to 2.6 V.

Acknowledgements

This work was financially supported by the National Key Research and Development Program of China [Grant Number 2021YFB2400300], National Natural Science Foundation of China [Grant Number 21875195, 22021001], Fundamental Research Funds for the Central Universities [Grant Number 20720190040], and The Key Project of Science and Technology of Xiamen [Grant Number 3502Z20201013]. We were also grateful for the technical support provided by Center for Micro-nano Fabrication and Advanced Characterization of Tan Kah Kee Innovation Laboratory in FE-SEM, XPS, and NMR spectroscopy.

Conflicts of interest

There are no conflicts of interest to declare.

Keywords: Lithium ion conductor • Lithium-sulfur battery • $Li_7La_3Zr_2O_{12}$ (LLZO) • Nafion • Shuttle effect

[1] a) J. B. Goodenough, Y. Kim, *Chem. Mater.* **2009**, *22*, 587-603; b) J. M. Tarascon, M. Armand, *Nature* **2001**, *414*, 359-367; c) W. He, W. Guo, H. Wu, L. Lin, Q. Liu, X. Han, Q. Xie, P. Liu, H. Zheng, L. Wang, X. Yu, D. L. Peng, *Adv. Mater.* **2021**, *33*, e2005937.

[2] a) P. G. Bruce, S. A. Freunberger, L. J. Hardwick, J. M. Tarascon, *Nat. Mater.* **2011**, *11*, 19-29; b) X. Tao, J. Wang, C. Liu, H. Wang, H. Yao, G. Zheng, Z. W. Seh, Q. Cai, W. Li, G. Zhou, C. Zu, Y. Cui, *Nat. Commun.* **2016**, *7*, 11203; c) S. H. Chung, C. H. Chang, A. Manthiram, *Adv. Funct. Mater.* **2018**, *28*, 1801188; d) Y. Chen, T. Wang, H. Tian, D. Su, Q. Zhang, G. Wang, *Adv. Mater.* **2021**, *33*, e2003666.

[3] a) D.-W. Wang, Q. Zeng, G. Zhou, L. Yin, F. Li, H.-M. Cheng, I. R. Gentle, G. Q. M. Lu, *J. Mater. Chem. A* **2013**, *1*, 9382-9394; b) G. Li, S. Wang, Y. Zhang, M. Li, Z. Chen, J. Lu, *Adv. Mater.* **2018**, *30*, e1705590; c) Y. Z. Wang, X. X. Huang, S. Q. Zhang, Y. L. Hou, *Small Methods* **2018**, *2*, 1700345; d) T. Tang, Y. Hou, *Small Methods* **2019**, *4*, 1900001; e) P. Wang, B. Xi, M. Huang, W. Chen, J. Feng, S. Xiong, *Adv. Energy Mater.* **2021**, *11*, 2002893.

[4] a) X. Liang, Z. Y. Wen, Y. Liu, M. F. Wu, J. Jin, H. Zhang, X. W. Wu, *J. Power Sources* **2011**, *196*, 9839-9843; b) S. S. Zhang, J. A. Read, *J. Power Sources* **2012**, *200*, 77-82; c) F. Wu, J. T. Lee, N. Nitta, H. Kim, O. Borodin, G. Yushin, *Adv. Mater.* **2015**, *27*, 101-108; d) M. Zhao, B. Q. Li, X. Q. Zhang, J. Q. Huang, Q. Zhang, *ACS Cent. Sci.* **2020**, *6*, 1095-1104.

[5] a) Z. Li, J. Zhang, X. W. D. Lou, *Angew. Chem. Int. Ed.* **2015**, *127*, 13078-13082; b) Y. Peng, B. Li, Y. Wang, X. He, J. Huang, J. Zhao, *ACS* Appl. *Mater. Interfaces* **2017**, *9*, 4397-4403; c) P. M. Xin, B. Jin, H. Li, X. Y. Lang, C. C. Yang, W. Gao, Y. F. Zhu, W. Q. Zhang, S. X. Dou, Q. Jiang, *ChemElectroChem* **2017**, *4*, 115-121; d) C. Li, Z. Xi, D. Guo, X. Chen, L. Yin, *Small* **2018**, *14*, 1701986.

[6] a) G. Zhou, D.-W. Wang, F. Li, P.-X. Hou, L. Yin, C. Liu, G. Q. Lu, I. R. Gentle, H.-M. Cheng, *Energy Environ. Sci.* **2012**, *5*, 8901-8906; b) N. Jayaprakash, J. Shen, S. S. Moganty, A. Corona, L. A. Archer, *Angew. Chem. Int. Ed.* **2011**, *50*, 5904-5908; c) W. D. Zhou, C. M. Wang, Q. L. Zhang, H. D. Abruna, Y. He, J. W. Wang, S. X. Mao, X. C. Xiao, *Adv. Funct. Mater.* **2015**, *5*, 1401752; d) H. J. Peng, W. T. Xu, L. Zhu, D. W. Wang, J. Q. Huang, X. B. Cheng, Z. Yuan, F. Wei, Q. Zhang, *Adv. Funct. Mater.* **2016**, *26*, 6351-6358; e) W. C. Du, Y. X. Yin, X. X. Zeng, J. L. Shi, S. F. Zhang, L. J. Wan, Y. G. Guo, *ACS Appl. Mater. Interfaces* **2016**, *8*, 3584-3590; f) W. Y. Li, Z. Y. Zhang, W. P. Kang, Y. B. Tang, C. S. Lee, *ChemElectroChem* **2016**, *3*, 999-1005; g) L. Carbone, J. Peng, M. Agostini, M. Gobet, M. Devany, B. Scrosati, S. Greenbaum, J. Hassoun, *ChemElectroChem* **2017**, *4*, 209-215; h) S. Y. Li, W. P. Wang, H. Duan, Y. G. Guo, *J. Energy Chem.* **2018**, *27*, 1555-1565; i) X. Hong, R. Wang, Y. Liu, J. Fu, J. Liang, S. Dou, *J. Energy Chem.* **2020**, *42*, 144-168.

[7] a) J. Q. Huang, Q. Zhang, F. Wei, *Energy Stor. Mater.* **2015**, *1*, 127-145; b) L. L. Fan, M. Li, X. F. Li, W. Xiao, Z. W. Chen, J. Lu, *Joule* **2019**, *3*, 361-386; c) L. Chen, H. Yu, W. Li, M. Dirican, Y. Liu, X. Zhang, *J. Mater. Chem. A* **2020**, *8*, 10709-10735.

[8] a) Y. Xiang, J. Li, J. Lei, D. Liu, Z. Xie, D. Qu, K. Li, T. Deng, H. Tang, ChemSusChem **2016**, *9*, 3023-3039; b) Z. Wei, Y. Ren, J. Sokolowski, X. Zhu, G. Wu, *InfoMat* **2020**, *2*, 483-508; c) S. Li, W. Zhang, J. Zheng, M. Lv, H. Song, L. Du, *Adv. Energy Mater.* **2020**, *11*, 2000779.

[9] a) S. H. Chung, A. Manthiram, *Adv. Funct. Mater.* **2014**, *24*, 5299-5306; b) J. Q. Huang, T. Z. Zhuang, Q. Zhang, H. J. Peng, C. M. Chen, F. Wei, *ACS Nano* **2015**, *9*, 3002-3011; c) J. D. Zhu, Y. Q. Ge, D. Kim, Y. Lu, C. Chen, M. J. Jiang, X. W. Zhang, *Nano Energy* **2016**, *20*, 176-184; d) S. H. Chung, P. Han, R. Singhal, V. Kalra, A. Manthiram, *Adv. Energy Mater.* **2015**, *5*, 1500738; e) X. Song, S. Q. Wang, G. P. Chen, T. Gao, Y. Bao, L. X. Ding, H. H. Wang, *Chem. Eng. J.* **2018**, *333*, 564-571; f) J. Liu, K. Li, Q. Zhang, X. Zhang, X. Liang, J. Yan, H. H. Tan, Y. Yu, Y. Wu, *ACS Appl. Mater. Interfaces* **2021**, *13*, 45547-45557; g) H. J. Peng, D. W. Wang, J. Q. Huang, X. B. Cheng, Z. Yuan, F. Wei, Q. Zhang, *Adv. Sci.* **2016**, *3*, 1500268; h) T. Y. Lei, W. Chen, W. Q. Lv, J. W. Huang, J. Zhu, J. W. Chu, C. Y. Yan, C. Y. Wu, Y. C. Yan, W. D. He, J. Xiong, Y. R. Li, C. L. Yan, J. B. Goodenough, X. F. Duan, *Joule* **2018**, *2*, 2091-2104; i) C. Chen, Q. B. Jiang, H. F. Xu, Y. P. Zhang, B. K. Zhang, Z. Y. Zhang, Z. Lin, S. Q. Zhang, *Nano Energy* **2020**, *76*, 105033; j) S. Ali, C. Tan, M. Waqas, W. Q. Lv, Z. H. Wei, S. H. Wu, B. Boateng, J. N. Liu, J. Ahmed, J. Xiong, J. B. Goodenough, W. D. He, *Adv. Mater. Interfaces* **2018**, *5*, 1701147; k) J. H. Ahn, T. S. You, S. M. Lee, D. Esken, D. Dehe, Y. C. Huang, D. W. Kim, *J. Power Sources* **2020**, *472*, 228519; l) J. Balach, T. Jaumann, S. Muhlenhoff, J. Eckert, L. Giebeler, *Chem. Commun.* **2016**, *52*, 8134-8137; m) C. Li, P. Zhang, J. H. Dai, X. Shen, Y. Y. Peng, Y. Y. Zhang, J. B. Zhao, *ChemElectroChem* **2017**, *4*, 1535-1543; n) I. Bauer, S. Thieme, J. Brückner, H. Althues, S. Kaskel, *J. Power Sources* **2014**, *251*, 417-422; o) T. Z. Zhuang, J. Q. Huang, H. J. Peng, L. Y. He, X. B. Cheng, C. M. Chen, Q. Zhang, *Small* **2016**, *12*, 381-389; p) J. Wang, P. Zhai, T. Zhao, M. Li, Z. Yang, H. Zhang, J. Huang, *Electrochim. Acta* **2019**, *320*, 134558.

[10] a) Z. Lin, Z. Liu, N. J. Dudney, C. Liang, *ACS Nano* **2013**, *7*, 2829-2833; b) Z. Lin, C. Liang, *J. Mater. Chem. A* **2015**, *3*, 936-958; c) F. Han, J. Yue, X. Fan, T. Gao, C. Luo, Z. Ma, L. Suo, C. Wang, *Nano Lett.* **2016**, *16*, 4521-4527; d) D. N. Lei, K. Shi, H. Ye, Z. P. Wan, Y. Y. Wang, L. Shen, B. H. Li, Q. H. Yang, F. Y. Kang, Y. B. He, *Adv. Funct. Mater.* **2018**, *28*, 1707570; e) M. Zhao, B. Q. Li, H. J. Peng, H. Yuan, J. Y. Wei, J. Q. Huang, *Angew. Chem. Int. Ed.* **2020**, *59*, 12636-12652.

[11] a) A. K. Baral, S. Narayanan, F. Ramezanipour, V. Thangadurai, *Phys.* Chem. *Chem. Phys.* **2014**, *16*, 11356-11365; b) A. J. Samson, K. Hofstetter, S. Bag, V. Thangadurai, *Energy Environ. Sci.* **2019**, *12*, 2957-2975; c) B. Gao, R. Jalem, H. K. Tian, Y. Tateyama, *Adv. Energy Mater.* **2021**, *12*, 2102151.

[12] a) F. D. Han, Y. Z. Zhu, X. F. He, Y. F. Mo, C. S. Wang, *Adv. Energy Mater.* **2016**, *6*, 1501590; b) W. Q. Zhang, J. H. Nie, F. Li, Z. L. Wang, C. Q. Sun, Nano *Energy* **2018**, *45*, 413-419; c) D. Xu, J. Su, J. Jin, C. Sun, Y. Ruan, C. Chen, Z. Wen, *Adv. Energy Mater.* **2019**, *9*, 1900611; d) D. Zhou, M. Y. Zhang, F. Sun, T. Arlt, J. E. Frerichs, K. Dong, J. Wang, A. Hilger, F. Wilde, M. Kolek, M. R. Hansen, P. Bieker, I. Manke, M. C. Stan, M. Winter, *Nano Energy* **2020**, *77*, 105196; e) F. Peng, S. Li, T. Geng, C. Li, S. Zeng, *J. Electrochem.* **2020**, *26*, 308-314.

[13] a) Z. Q. Jin, K. Xie, X. B. Hong, Z. Q. Hu, X. Liu, *J. Power Sources* 2012, *218*, 163-167; b) J.-Q. Huang, Q. Zhang, H.-J. Peng, X.-Y. Liu, W.-Z. Qian, F. Wei, *Energy Environ. Sci.* **2014**, *7*, 347-353; c) X. Yu, J. Joseph, A. Manthiram, *J. Mater. Chem. A* **2015**, *3*, 15683-15691; d) J. Gao, Q. J. Shao, J. Chen, *J. Energy Chem.* **2020**, *46*, 237-247.

[14] a) S. Sachan, C. A. Ray, S. A. Perusich, *Polym. Eng. Sci.* **2002**, *42*, 1469-1480; b) J. Gao, C. S. Sun, L. Xu, J. Chen, C. Wang, D. C. Guo, H. Chen, *J. Power Sources* **2018**, *382*, 179-189.

[15] a) H. Z. Zhang, H. M. Zhang, X. F. Li, Z. S. Mai, W. P. Wei, Y. Li, *J. Power Sources* **2012**, *217*, 309-315; b) Z. Q. Jin, K. Xie, X. B. Hong, *J. Mater. Chem. A* **2013**, *1*, 342-347.

[16] H. Huo, J. Luo, V. Thangadurai, X. Guo, C.-W. Nan, X. Sun, *ACS Energy Lett.* **2019**, *5*, 252-262.

[17] K. Z. Walle, L. Musuvadhi Babulal, S. H. Wu, W. C. Chien, R. Jose, S. J. Lue, J. K. Chang, C. C. Yang, *ACS Appl. Mater. Interfaces* **2021**, *13*, 2507-2520.

[18] a) X. Wang, H. M. Hua, L. Q. Peng, B. Y. Huang, P. Zhang, J. B. Zhao, *Appl. Surf. Sci* **2021**, *542*, 148661; b) B. Y. Huang, H. M. Hua, L. Q. Peng, X. Wang, X. Shen, R. Y. Li, P. Zhang, J. B. Zhao, *J. Power Sources* **2021**, *498*, 229908.

[19] a) G. Zhang, H. J. Peng, C. Z. Zhao, X. Chen, L. D. Zhao, P. Li, J. Q. Huang, Q. Zhang, *Angew. Chem. Int. Ed.* **2018**, *57*, 16732-16736; b) X. N. Li, J. W. Liang, W. H. Li, J. Luo, X. Li, X. F. Yang, Y. F. Hu, Q. F. Xiao, W. Q. Zhang, R. Y. Li, T. K. Sham, X. L. Sun, *Chem. Mater.* **2019**, *31*, 2002-2009.

[20] F. Y. Shen, M. B. Dixit, X. H. Xiao, K. B. Hatzell, *ACS Energy Lett.* **2018**, *3*, 1056-1061.

[21] a) Y. H. Huang, R. Field, Q. Chen, Y. D. Peng, M. S. Walczak, H. Zhao, G. Y. Zhu, Z. Liu, L. Li, *Commun. Chem.* **2019**, *2*, 1-8; b) S. Nanda, A. Manthiram, *Energy Environ. Sci.* **2020**, *13*, 2501-2514.

[22] a) Z. Wang, W. Huang, J. Hua, Y. Wang, H. Yi, W. Zhao, Q. Zhao, H. Jia, B. Fei, F. Pan, *Small Methods* **2020**, *4*, 2000082; b) S. Xia, X. Zhang, G. Yang, L. Shi, L. Cai, Y. Xia, J. Yang, S. Zheng, *ACS Appl. Mater. Interfaces* **2021**, *13*, 11920-11929.

[23] Y. Liu, H. Liu, Y. Lin, Y. Zhao, H. Yuan, Y. Su, J. Zhang, S. Ren, H. Fan, Y. Zhang, *Adv. Funct. Mater.* **2021**, *31*, 2104863.

[24] a) G. M. Zhou, Y. B. Zhao, C. X. Zu, A. Manthiram, *Nano Energy* **2015**, *12*, 240-249; b) N. Moreno, Á. Caballero, J. Morales, E. Rodríguez-Castellón, *J. Power Sources* **2016**, *313*, 21-29.

[25] a) K. A. See, M. Leskes, J. M. Griffin, S. Britto, P. D. Matthews, A. Emly, A. Van der Ven, D. S. Wright, A. J. Morris, C. P. Grey, R. Seshadri, *J. Am. Chem. Soc.* **2014**, *136*, 16368-16377; b) L. A. Huff, J. L. Rapp, J. A. Baughman, P. L. Rinaldi, A. A. Gewirth, *Surf. Sci.* **2015**, *631*, 295-300.

[26] L. H. Abrha, T. T. Hagos, Y. Nikodimos, H. K. Bezabh, G. B. Berhe, T. M. Hagos, C. J. Huang, W. A. Tegegne, S. K. Jiang, H. H. Weldeyohannes, S. H. Wu, W. N. Su, B. J. Hwang, *ACS Appl. Mater. Interfaces* **2020**, *12*, 25709-25717.

[27] H. N. Zhang, J. J. Pan, X. C. He, M. Pan, *J. Appl. Polym. Sci.* **2008**, *107*, 3306-3309.

10.1002/celc.202200416

Entry for the Table of Contents

ARTICLE

To suppress the shuttle effect of polysulfides, the strategy of constructing a single-ion conductive layer on the separator was used. By a simple coating method, a dense and ion-selective layer was prepared with LLZO and Li-Nafion. Correspondingly, the lithium ion transport number achieves 0.79, and the lithium-sulfur batteries have better lithium deposition behavior and cycling performances.

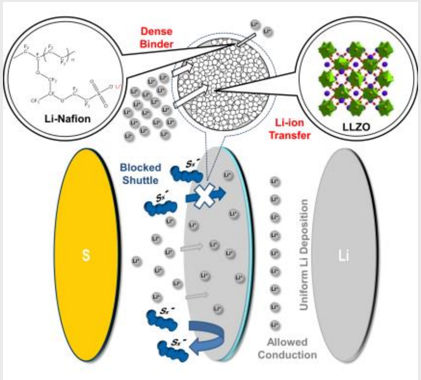

Boyang Huang, Haiming Hua, Pengbin Lai, Xiu Shen, Ruiyang Li, Zheng He, Peng Zhang, Jinbao Zhao**

Page 1 – Page 10

Constructing Ion-Selective Coating Layer with Lithium Ion Conductor LLZO and Binder Li-Nafion for Separator Used in Lithium-Sulfur Batteries